Journal Pre-proofs

Ultrahigh nanostructured drug payloads from degradable mesoporous silicon aerocrystals

D. Nadarassan, A. Loni, L.T. Canham, N. Scoutaris, V. Trivedi, D. Douroumis

PII: S0378-5173(21)00645-1
DOI: https://doi.org/10.1016/j.ijpharm.2021.120840
Reference: IJP 120840

To appear in: *International Journal of Pharmaceutics*

Received Date: 4 May 2021
Revised Date: 27 June 2021
Accepted Date: 28 June 2021

Please cite this article as: D. Nadarassan, A. Loni, L.T. Canham, N. Scoutaris, V. Trivedi, D. Douroumis, Ultrahigh nanostructured drug payloads from degradable mesoporous silicon aerocrystals, *International Journal of Pharmaceutics* (2021), doi: https://doi.org/10.1016/j.ijpharm.2021.120840

Ultrahigh nanostructured drug payloads from degradable mesoporous silicon aerocrystals

D. Nadarassan[1], A. Loni[1], L. T. Canham[1,4*], N. Scoutaris[2], V. Trivedi[3*] , D. Douroumis[2]

[1]pSiMedica Ltd, Malvern Hills Science Park, Geraldine Road, Malvern, Worcestershire, WR14 3SZ, UK

[2]Faculty of Engineering of Science, University of Greenwich, Central Avenue, Chatham Maritime, Kent ME4 4TB, UK

[3]Medway School of Pharmacy, University of Kent, Medway Campus, Central Avenue, Chatham Maritime, Chatham, Kent ME4 4TB, United Kingdom

[4]School of Physics and Astronomy, University of Birmingham, Edgbaston, Birmingham B15 2TT, United Kingdom

Abstract

* **V. Trivedi**, Medway School of Pharmacy, University of Kent, Medway Campus, Central Avenue, Chatham Maritime, Chatham, Kent ME4 4TB, United Kingdom

*__L.T. Canham__, School of Physics and Astronomy, University of Birmingham, Edgbaston, Birmingham B15 2TT, United Kingdom

Porous silicon has found increased attention as a drug delivery system due to its unique features such as high drug payloads, surface area and biodegradation. In this study supercritical fluid (SCF) assisted drying of ultrahigh porosity (> 90%) silicon particles and flakes was shown to result in much higher mesopore volumes (~ 4.66 cm^3/g) and surface areas (~ 680 m^2/g) than with air-drying. The loading and physical state of the model drug (S)-(+)-Ibuprofen in SCF dried matrices was quantified and assessed using thermogravimetric analysis, differential scanning calorimetry, UV-Vis spectrophotometry, gravimetric analysis, gas adsorption and electron microscopy. Internal drug payloads of up to 72% were achieved which was substantially higher than values published for both conventionally dried porous silicon (17-51%) and other mesoporous materials (7-45%). *In-vitro* degradability kinetics of SCF-dried matrices in simulated media was also found to be faster than air-dried controls. The *in-vitro* release studies provided improved but sustained drug dissolution at both pH 2.0 and pH 7.4

Keywords: Porous silicon, Ibuprofen, Supercritical fluid, Controlled release, degradable.

1 Introduction

Mesoporous materials are receiving increasing attention for drug delivery due to their biocompatibility and controlled morphology (e.g., pore size and surface area) [1-3]. Moreover, the ability to tune the delivery of therapeutic levels of drug substances by restricted diffusion, matrix biodegradation, or combination of both make these materials highly attractive in the development of controlled release formulations.

Drug loading level in mesoporous materials is one of the most important key parameters to achieve required release and drug concentration in the blood after administration. Reservoir systems for drug delivery typically achieve higher payloads than matrix systems but can suffer from "dose dumping". Matrix systems that are mesoporous and biodegradable can minimise such risks and provide controlled delivery of the drugs entrapped within**.** One of the limitations of using mesoporous materials in drug delivery is the inadequate drug loading which is largely dependent on the type of particles along with pore sizes and volumes. There are several studies where porous materials such as silica nanoparticles (MCM-41, SBA-13) [4,5], anodised silicon (pSi) [6] or carbon [7] with pore volumes ranging from 0.5 – 2.2 cm^3/g have been used successfully for drug loadings varying from 10 – 40%.

This variability in drug loading level usually corresponds to the properties of a given matrix such as the pore volume and/or porosity but high porosity doesn't always result into improved drug loading. For example, silica aerogels can have extremely high pore volumes (*e.g.* 2-10 cm^3/g) but drug loading levels have generally remained limited to 10-40 wt% due to issues related to their mechanical integrity upon exposure to a liquid during the drug entrapment procedure [8]. This issue can be addressed by the application of SCFs but the relatively low solubility of pharmaceuticals in common solvents such as supercritical carbon dioxide ($scCO_2$) can be a limiting factor in achieving the desire drug loading into a mesoporous matrix [5, 9].

Mesoporous materials such as aerogels have gained significant interest especially as drug delivery systems due to their unique properties such as the high specific area and the increased drug loading capabilities [10]. In addition, the drug encapsulation in the porous network facilitates the transformation of the drug into a stable amorphous state and results in increased dissolution rates of water insoluble active pharmaceutical ingredients (APIs). As silicon aerogels come in contact with gastrointestinal fluids the penetration of the liquids causes the destruction of the porous network due to the created sizable capillary forces.

Trucillo et al by using supercritical CO_2 entrapped ampicillin loaded liposomes in alginate aerogels with the aim to create a meta – carrier [11]. The authors found that the nanoporous structure of alginate gels was well preserved by CO_2 drying while the ampicillin release rates from the meta – carriers were doubled compared to liposome nanoparticles. In general CO_2 has been successfully used for processing of liposome drug delivery systems [12-14]. The CO_2 absorption was used to encapsulated anti - inflammatory active substances (NSAIDs) in maize

starch (MSA) and calcium alginate aerogels (CAA) respectively [15]. The biopolymer aerogels were found to possess different effect on the drug dissolution rates with MSA featuring faster release rates while CAA facilitated a controlled release manner for the NSAIDs.

A $scCO_2$ – foamed aerogel comprising of silk fibroin as cell adhesion promoter and poly(e-caprolactone) as biopolymeric matrix loaded with dexamethasone (DX) or the salt (DS) for bone regeneration was recently reported [16,17] The drug form showed differences in the release rates while the scaffolds fulfilled the required properties such as porosity, pore size distribution and interconnectivity which are required for bone repair. *In vivo* animal trials revealed the importance of the drug selection in promoting bone regeneration where several formulations presented increased number of ossification foci. There are several studies where aerogels have been used for drug loading applications [18 – 20], cosmetics [21], catalysis [22], sound absorption and many other applications [23 – 28]. Similarly, $scCO_2$ has been employed in producing cyclodextrin complexes with BCS II drug for solubility improvement [29-31]. For example, Benznidazole complexation in γ-cyclodextrin resulted in significantly higher drug dissolution in comparison to the drug alone. The application of $scCO_2$ in performing solvent-free encapsulation is also very common e.g. ketamine-loaded porous silicon particles led to sustained drug release after encapsulation in poly(lactic-co-glycolic acid) [32].

In this regard, the use of aerocrystals with high porosity is of great interest [33, 34]. Aerocrystals (crystalline matrices of greater than 85% porosity) have similar surface areas and pore volumes to the more common amorphous “aerogels” but markedly different morphologies and mechanical properties. This can result in differing drug loading levels achievable, particularly if the mechanical strength of the matrix differs appreciably. However, conventional drying methods usually result in collapsed pores and lower porosity than expected. Novel methods such as $scCO_2$ assisted drying can overcome issues associated to conventional methods as it is benign and has excellent miscibility with commonly used organic solvent which can allow efficient drying of aerocrystals without compromising the resultant porosity [35].

This work discusses the $scCO_2$ drying of aerocrystals and its effect on the resultant porosity and surface area when compared to the oven-dried samples. Furthermore, we investigated the drug loading capacity of the aerocrystals with the highest surface area and the dissolution

rates of ibuprofen as model active substance. The drug loading was performed by the melt-intrusion method to achieve quick and uniform drug loading into the porous aerocrystals [36].

2 Materials and Methods

2.1 Materials

3-aminopropyltriethoxysilane (APTES), 3-aminopropyltriethoxysilane (APDMES) and (S)-(+)-Ibuprofen (IBU) were purchased from Sigma Aldrich, UK. Liquid carbon dioxide with 99.9% purity was supplied from BOC Ltd., UK. All other solvents and buffers also obtained from Sigma Aldrich, UK and were research-grade chemicals.

2.2 Methods

2.2.1 Manufacturing

Porous silicon aerocrystal layers were prepared according to the method described by Canham et al [33]. Briefly, aerocrystals synthesis was performed on 150 mm diameter p-type wafers (resistivity range 0.005-0.02 Ω.cm) by electrochemical anodisation in hydrofluoric acid/methanol-based electrolyte mixture to obtain 200 µm silicon layers of high porosity (> 85%). Each layer was partially detached from the wafer immediately after anodisation via high current density pulse and transferred to methanol bath. The layer fragments were kept wet throughout detachment and transfer to methanol was done immediately to avoid air-drying which can result in the collapse of highly porous structures. The wet fragments were rinsed several times using fresh methanol to minimise residual hydrofluoric acid and were stored thereafter in absolute ethanol until scCO_2 drying.

2.2.1 Supercritical carbon dioxide drying of aerocrystals

scCO_2 drying was carried out using a Quorum Technologies Ltd K850 dryer. 1 g of aerocrystal was transferred directly from ethanol storage to the drying chamber. As the first step, drying chamber was continuously flushed with liquid CO_2 to replace ethanol in pores with CO_2. Each flushing step comprised of stirring for 4 min, with a static 1 min soak followed by partially emptying the chamber and replenishing it with fresh CO_2. The presence of ethanol in the CO_2 stream was determined visually at the chamber outlet, as evinced by the presence of a damp

patch on filter paper. This first step was repeated 10 times to remove majority of ethanol from aerocrystals. The temperature of the high-pressure vessel was then increased to 32 °C for $scCO_2$ drying to commence at 1100 psi in the second step. Equivalent air-dried samples (dried at room temperature on removal from the ethanol storage) were used as controls.

2.2.2 Surface Passivation

The internal surface area of as-anodised porous silicon is terminated with chemically reactive, hydrophobic Si-H_x bonds (x=1,2,3). To obtain a low-reactivity internal surface, each $scCO_2$ dried sample was thermally oxidised at 600 °C for 16 h in a mixture of oxygen and nitrogen (1:99), which also rendered them hydrophilic.

2.2.3 Porosity, Surface Area and Pore Volume Measurements

The gravimetric porosity was calculated using the weight of the porous silicon, along with the density of bulk silicon and the total weight loss due to anodisation. Nitrogen gas adsorption/desorption [36] was carried out using a Micromeritics *Tristar 3000*. The samples were degassed under flowing nitrogen at 90 °C for 1 h before analysis. Computational analysis of the isotherms yielded absolute values for surface area (based on the Brunauer-Emmett-Teller (BET) method), pore volume (based on the Barrett-Joyner-Halenda (BJH) adsorption method, with P/P_o chosen to represent the maximum available pore volume) and average pore diameter (from single-point adsorption). From the pore volume, the average porosity was calculated and compared with the gravimetric value.

Thermoporometry, was also used to confirm the pore volume and pore diameter of aerocrystals. The technique determines pore size based on the melting or crystallization point depression of a liquid confined within pores. 3-5 mg of sample was hermetically sealed into aluminium pans for the differential scanning calorimeter (DSC) analysis. The temperature shifts was measured using DSC for cyclohexane exothermic freezing and endothermic melting within the temperature range of -45°C to 10 °C, at a heating rate of 0.5 °C/min under N_2 gas purge of 60 mL/min.

2.3 Ibuprofen Loading

Drug loading was performed only on the $scCO_2$-dried aerocrystals. Dried aerocrystals were gently hand-milled using pestle and mortar prior to IBU loading by the melt-intrusion method [36]. Briefly, 1.4 g of IBU was melted on a hot plate at 70 °C and then 0.5 g of aerocrystals of preferred aerocrystals was slowly added under constant stirring to ensure a homogeneous mix of the drug within the porous particles. The drug adsorption in melt-intrusion method occurs as a result of strong capillary action generated within the mesopores. The formulation was allowed to cool to room temperature and gently ground using mortar and pestle to separate agglomerated particles and stored at room temperature in a sealed vial. The drug loading was determined after 6 weeks of storage to ensure complete drug recrystallization before the analysis.

The presence of drug was also studied using cross-sectional SEM/EDX analysis. Individual aerocrystal flakes were immersed in molten IBU for 10 min at 50 °C to facilitate drug ingress into the porous material. Both sides of the flakes were wiped carefully with a filter paper after the removal from the melt followed by methanol-soaked swabs to remove the surface adsorbed ibuprofen.

2.4 Drug Payload Evaluation

2.4.1 Theoretical maximum payload based on porosity

The maximum theoretical drug payload was calculated based on the crystalline density of the model drug (ρ_{drug} = 1.093 g/cm^3) and accessible pore volume of porous silicon (V_{pSi}) as shown below:

$$\boldsymbol{Payload} = \left[\frac{\boldsymbol{V_{pSi} \times \rho_{drug}}}{\boldsymbol{1 + V_{pSi} \times \rho_{drug}}}\right] \times \boldsymbol{100} \quad \text{(Eq 1)}$$

The theoretical payloads were compared with the experimental data generated by N_2 adsorption, TGA, UV spectroscopy, and HPLC.

2.4.2 Payload via N_2 Adsorption Data

The drug loading (%w/w) via N_2 adsorption data was calculated from BJH pore volume of empty and loaded V_{loaded}) aercrystal particles using the following equation:

$$DL = \left[\frac{(V_{pSi} - V_{loaded}) \times \rho_{drug}}{1 + V_{pSi} \times \rho_{drug}}\right] \quad \text{(Eq 2)}$$

2.4.3 Payload via Thermal Analysis

Thermogravimetric analysis (TGA) was carried out by heating the formulation at 10 °C/min to 500°C under a constant flow of N_2 (50 mL/min) and the weight loss was monitored. For DSC, the 3-5 mg of sample was loaded into a hermetically sealed aluminium pan and heated from -80 to 70 °C at a heating rate of 10 °C/min under N_2 flow (60 mL/min). The instrument was calibrated for the melting point and heat of fusion (T_m [°C] and ΔH_m [mJ mg^{-1}]) of Indium (156.6°C and 28.4mJ mg^{-1}).

2.4.4 Payload via UV-Vis Spectroscopy

An accurately weighed quantity (10 mg) IBU-loaded aerocrystals were dispersed in 10 mL of methanol, stirred at 500-700 rpm for 30 min, followed by sonication for 15 min to recover the drug from the aerocrystal matrix. The methanol solution was then diluted in 900 mL of phosphate buffer (pH 7.4) and analysed using a Shimadzu UV-160 (Shimadzu, Japan) at 214 nm to determine the IBU content in the media.

2.5 Qualitative Analysis of Loaded Drug

2.5.1 X-Ray Diffraction (XRD)

XRD was used to determine the solid state of the pure active substance, physical mixtures and extracted materials, using a Bruker D8 Advance in 2Θ mode. A Cu anode at 40 kV and 40 Ma, parallel beam Goebel mirror, 0.2 mm exit slit, LynxEye Position Sensitive Detector with 3° opening (LynxIris at 6.5 mm) and sample rotation at 15 rpm were used for the analysis. Each sample was scanned from 2 to 40° 2Θ with a step size of 0.02° 2Θ and a counting time of 0.1 seconds per step.

2.5.2 Plan-View Scanning Electron Microscopy (SEM)

The SEM micrographs of powders were obtained using Hitachi SU8030 electron microscope (Hitachi, Tokyo, Japan. The samples were placed on a double-sided carbon adhesive tabs and coated with an ultrathin layer of carbon to minimize charging. The surface morphology of the loaded porous silicon was evaluated using a nominal magnification of 1000 (area = 0.012 mm^2) and higher magnifications were used to probe the morphology of any surface deposits. The accelerating voltage of the incident electron beam was set at 8 kV. This value was selected in order to minimize sample damage by the beam while maintaining adequate excitation.

2.5.3 Atomic Force Microscopy (AFM)

AFM analysis was performed on tapping mode using an easyscan 2 microscope (Nanosurf, Switzerland) and Tap 190Al-G cantilevers (BudgetSensors, Sofia, Bulgaria). The drive amplitude and the relative set point were chosen in a way that the intermittent force between the oscillated tip and the substrate would be minimum. The analysis of the images was performed using Nanosurf Eeasyscan software (Image Metrology, Hørsholm, Denmark). Statistical analysis was performed by using R statistics.

2.5.4 Cross-Sectional SEM/EDX

The internal spatial distribution of loaded drug was evaluated with a Hitachi 4800 Mk2 HRSEM (Hitachi, Tokyo, Japan). Aerocrystal flakes were freshly cleaved prior to analysis and the spectra were collected at 5 - 6 kV and processed using INCA software. Reference EDX spectra of pure drug available in powder form were also acquired to assess their stability under electron beam irradiation.

2.6 *In-vitro* degradability

The *in-vitro* degradability of aerocrystal flakes was determined by holding them in open platinum meshes in Tris buffer (50 mM) at pH 7.4 and 37 ^oC. Approximately 10 mg (±1.0 mg) of sample was suspended in TRIS buffer and 1.5 mL of sample was withdrawn at each time point. Sink conditions were maintained throughout the analysis and silicic acid generation was monitored by the molybedate blue assay over a period of 20 days [37]. The samples were stored at 4 ^oC till the time of analysis.

2.7 Drug Release Study

A USP type II Erweka DT 720 dissolution apparatus (Erweka, Hessen, Germany) was used to monitor the *in-vitro* dissolution profiles of IBU using the rotating basket method. Approximately 100 mg of drug-loaded aerocrystals was placed in each vessel containing 900 mL of dissolution media (phosphate buffer at pH 7.2 and 0.1 N HCl at pH 2). The dissolution media was equilibrated at 37 ± 0.5 °C at 100 rpm prior to introducing the drug containing flakes in the vessels. Samples were withdrawn at predetermined time intervals (10, 20, 30, 40, 50, 60, 80, 100 and 120 min) using a peristaltic pump attached to the dissolution apparatus and the drug release was quantified using a Shimadzu UV-160 spectrophotometer (Shimadzu, Tokyo, Japan) at 214 nm.

3 Results and Discussion

The electrochemical anodisation results in highly porous silicon wafer but conventional drying processes result in collapsing of the pores due to associated capillary forces during the solvent evaporation. Hence, silicon wafers were dried using $scCO_2$ to preserve the porous structures and specific surface area that can facilitate high drug loading in the matrix. The drying process in $scCO_2$ is governed by its effective mixing with the solvent in the pores followed by the gradual removal of the EtOH from the network. Initially, only convective mass transfer takes place due to the excess of EtOH in and around the wafers. The drying thereafter becomes diffusion controlled as the $scCO_2$ content in the pores increases until the complete removal of EtOH is achieved. Moreover, $scCO_2$ drying ensures that integrity of the network is not compromising during the drying process due to the lack of capillary forces responsible for collapsing the pores in conventional drying. Table 1 shows the nitrogen adsorption data for various air-dried and $scCO_2$-dried aerocrystals.

Table 1: Nitrogen gas adsorption and porosity data comparing air-dried and $scCO_2$-dried aerocrystals.

Sample	BET Surface Area (m^2/g)	Pore Volume (cm^3/g)	Average Pore Diameter (nm)	[a]Porosity (%)	[b]Porosity (%)
S1	*476*/491	*2.28*/3.01	*19.3*/24.6	*84.2*/87.5	88.8
S2	*441*/514	*2.32*/3.03	*21.1*/24.3	*84.4*/87.6	88.8
S3	*483*/525	*2.32*/3.15	*18.8*/23.9	*84.4*/88.0	89.8
S4	*484*/536	*2.29*/3.41	*18.6*/24.3	*84.2*/88.8	90.7
S5	*498*/534	*2.32*/3.40	*18.2*/27.0	*84.3*/88.8	92.1
S6	*560*/587	*2.18*/3.11	*15.4*/26.1	*83.5*/87.8	90.5
S7	*459*/536	*2.36*/3.31	*20.3*/24.6	*84.6*/88.5	89.3
S8	*543*/573	*2.39*/3.81	*17.8*/26.5	*84.8*/89.9	91.3
S9	*562*/591	*1.38*/3.68	*9.6*/28.0	*76.3*/89.5	92.3
S10	*562*/583	*1.82*/3.12	*12.5*/22.6	*80.9*/87.9	90.9
S11	*585*/592	*1.34*/3.05	*8.9*/23.5	*75.7*/87.6	93.0
S12	630	4.66	29.5	91.6	95.2
S13	681	3.96	23.0	90.2	96.7

*(*italicised data: air-dried equivalent*; [a] porosity from pore volume; [b] gravimetric porosity as calculated using aerocrystal weight, bulk silicon density and weight loss due to anodisation); the best two $scCO_2$-dried samples (S12 and S13) are included for reference.

The gas adsorption and gravimetric data (Table 1) confirm the advantage of $scCO_2$ drying over air-drying with respect to higher specific surface area, pore volume, total porosity and average pore size. The specific surface area of air-dried and $scCO_2$- dried samples ranged from 440-590 m^2/g and 630-680 m^2/g, respectively. Similarly, gravimetric pore volume of $scCO_2$-dried samples was as high as 97% in comparison to around 89-93% of air-dried samples. The average pore sizes of $scCO_2$-dried samples were also larger (23-30 nm) than the samples obtained after air-drying (*write the number once we know why we have two -three numbers for each sample*). Consistently higher specific surface area, pore volume, porosity and average pore size obtained from $scCO_2$-dried aerocrystals clearly indicate that the air-dried samples have been significantly compromised by the collapse of the porous network. The $scCO_2$-dried samples resulted in the porosities very close to the gravimetric values (Table 1), which suggested that there was no loss of porous network during or due to the drying process.

3.1 Drug Loading Studies

The drug loading in this work was performed via melt-intrusion process that involves displacement of air from the pores followed by complete and uniform pore filling by the melted drug [36]. This is a very simple and quick process to obtain desired drug loading into the porous flakes and, also does not lead to collapsed pores. The excess drug present on the surface can then be easily removed by simply wiping the surface off with a chosen solvent after the completion of drug loading process. The SEM micrographs presented in Fig. 1 of drug loaded aerocrystal flakes confirmed the absence of significant levels of drug on the surface of the nanostructure.

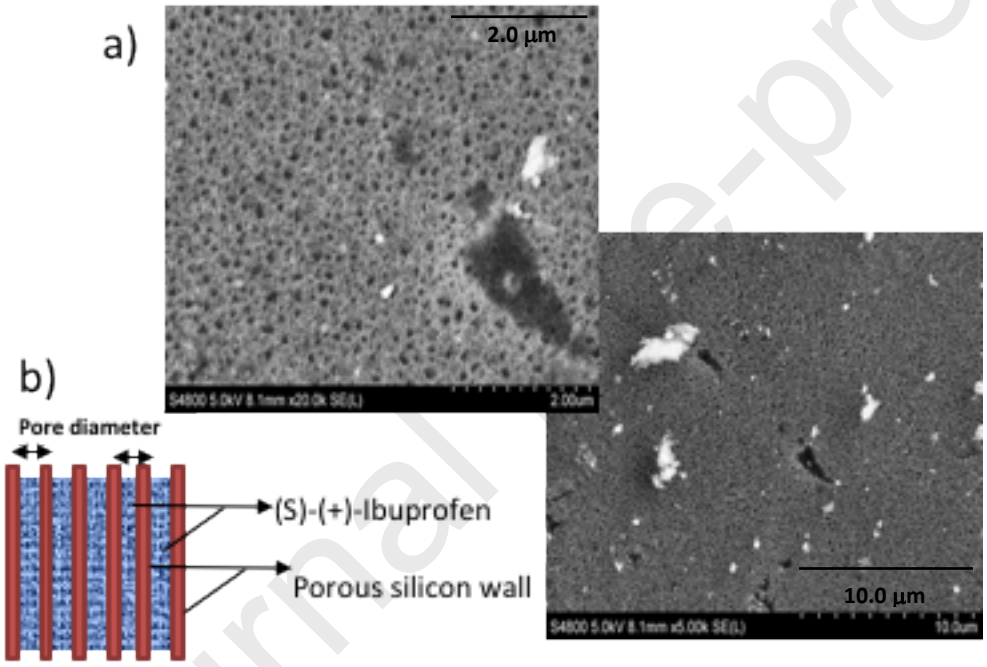

Fig. 1: a) SEM micrographs of ibuprofen melt loaded aerocrystal flakes and b) Schematic illustration of nanostructured porous silicon filled with (S)-(+)-ibuprofen

The surface area and pore volume values of pre- and post-loaded aerocrystals is presented in Table 2. The thermal oxidation of samples results in the reduction of surface area, pore volume and pore sizes as shown in table 2. Sample S6 (Table 1) was chosen for drug loading studies which had a surface area of 587 m^2/g, that reduced to 415 m^2/g after thermal oxidation. There were similar reductions in the pore volume and average pore diameter values from the pre-oxidation values. Such a decrease is likely to be attributed to the

expansion of the structure due to SiO_2 formation and/or significant expansion of the structure leading to obstruction of the pore openings.

The surface area and pore volume of aerocrystals reduced from 420 to 5.3 m^2/g and from 2.28 to 0.036 cm^3/g, respectively after ibuprofen loading. Reduction in the surface area and pore volume is a clear evidence of drug loading in the pores. However, unchanged pore diameter values could be due to the incomplete filling of the pores that may give access to N_2 adsorption during analysis as shown schematically in Fig. 1.

Table 2: Nitrogen gas adsorption data of thermally oxidised porous silicon and (S)-(+) Ibuprofen loaded aerocrystals.

Sample	BET Surface Area (m^2/g)	Pore Volume (cm^3/g)	Average Pore Diameter (nm)
Aerocrystals	420	2.28	25.9
IBU loaded aerocrystals	5.30	0.036	27.2

Fig. 2 presents the topographic and phase images of silicon aerocrystals with and without loaded IBU. The topographic AFM image demonstrates the roughness of the surface which is also is presented in the SEM results. Surface roughness were identified in the root mean square (RMS) value and was estimated to be 132.26 (±62) nm for the IBU loaded samples, and 30.43 (±18.13) nm for silica flakes. Moreover, a post-hoc Tukey test was applied (Fig. 3), where the mean RMS of drug loaded aerocrystals was found to be significantly different to the pure silica ($p=0.005$).

Also, the mean RMS of the pure silica powder and the flakes were not statistically different. The high RMS value of the IBU loaded aerocrystals was attributed to the drug loading process.. Furthermore, AFM also confirmed the homogeneous distribution of IBU in porous network and the absence of phase separation or evidence of crystalline material in any of the samples.

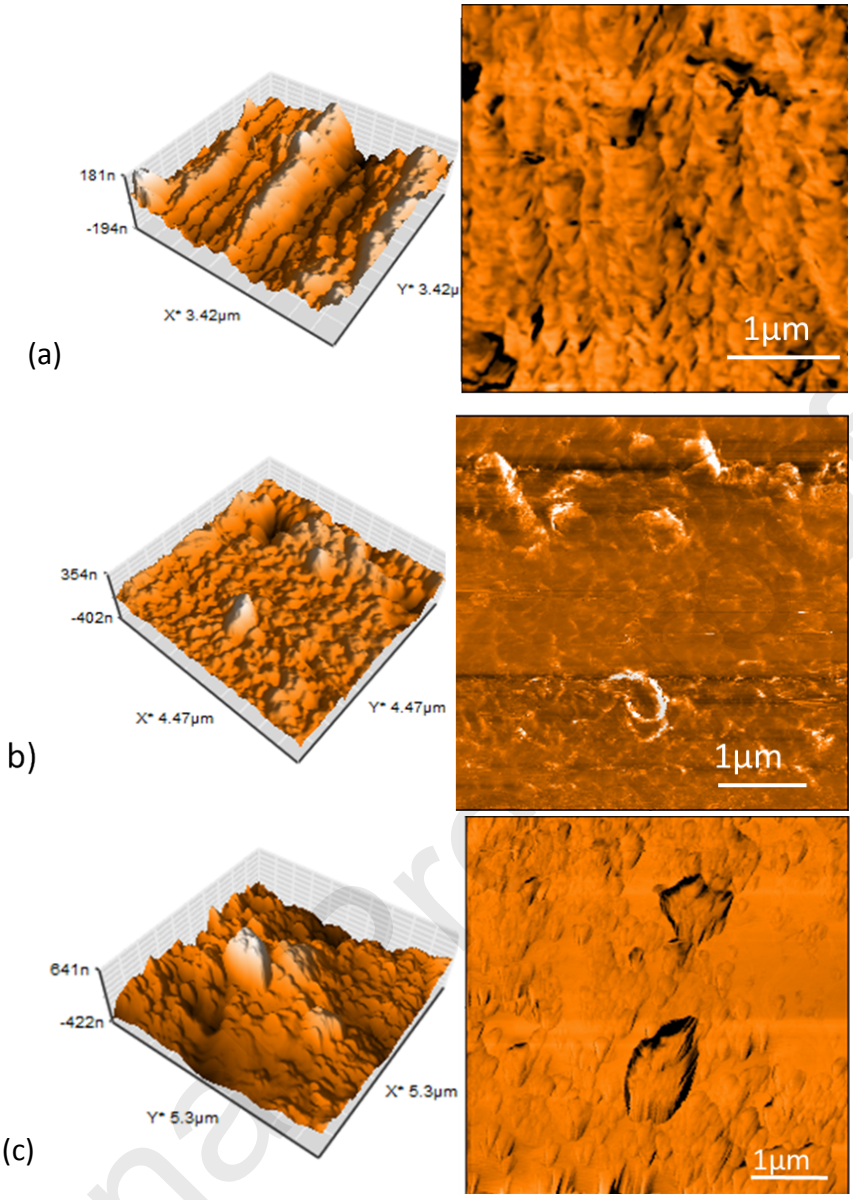

Fig 2: AFM of topographic and phase images of a) pSi powder, b) pSi flakes, cb) IBU loaded aerocrystal flakes.

Table 3 compares the IBU loading obtained using four experimental techniques and calculated value assuming complete pore filling with the drug of known density. The drug loading estimated via N_2 adsorption and UV methods were very close to the theoretical drug loading value of 71.2 wt%. A slightly higher IBU loading of 74.6 wt% was obtained with the TGA method due to the decomposition of both drug inside (IBU_{in}) and outside the pores (IBU_{out}).

Table 3: Drug payloads determined from different analytical methods.

Theoretical Payload (%w/w)	N_2 Adsorption (%w/w)	TGA (%w/w)	UV (%w/w)	DSC[a] (%Crystalline$_{out}$)	Drug in pores (%IBU$_{in}$)[c]
71.2	70.1	74.6	71.9	0.70[b]	73.9

[a] Unloaded crystallised drug outside the pores

[b] %Crystalline$_{out}$= ΔH_{bulk} x 100 / ΔH_{std}

[c] %IBU$_{in}$ = % IBU$_{total}$ (TGA) - % Crystalline$_{out}$

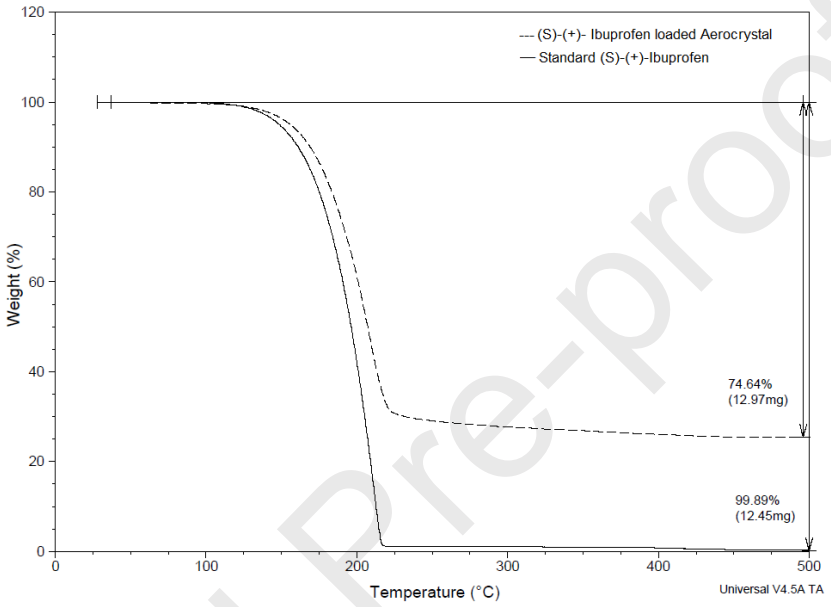

Fig. 3: TGA overlays for reference standard (S)-(+)-Ibuprofen and loaded (S)-(+)-Ibuprofen formulation

The physical state of the drug loaded in the pores was determined using DSC [38], which can differentiate between drug entrapped within mesopores and adsorbed to the outer surfaces. It is known that the drug confined in pores results in lower melting point than the drug present on the surface. The thermograms presented in Figure 4 showed two endothermic peaks corresponding to IBU confined in the pores at 29.4 °C the drug present outside 52.4 °C that matched with the melting temperature of standard IBU (52.5 °C).

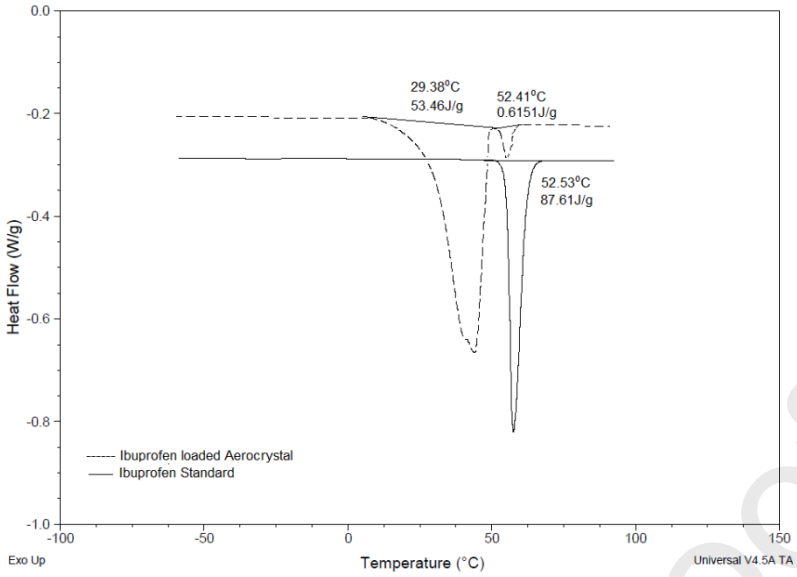

Fig. 4: Overlay DSC trace of standard reference IBU and loaded pSi.

The amount of drug, crystallinity and the relative quantities both inside and outside the mesopores were evaluated by DSC (Table 3). The Gibbs-Thomson equation describes the relationship between pore diameter and melting temperature depression, based on the fact that a depression in melting temperature is seen when a drug is confined in pores, where melting temperature depression inversely related to pore sizes [38]. This has also been observed in previous studies where the melting endotherm appears to shift to lower temperatures and presents lower enthalpy values [3, 39]. The amount of drug present outside was calculated from the ratio of the heat of fusion of bulk IBU (0.6151 J/g) and standard. The crystallinity values obtained were subtracted by the total drug load determined by TGA (Figure 3) to work out the drug present in the pores. The amount of the crystalline drug on the surface of the aerocrystals was calculated to be 7 mg/g.

3.2 Physical Characterisation of Loaded Drug

3.2.1 XRD

The physical state of the drug was also determined by XRD analysis. As shown in Figure 5 the bulk IBU presented high intensity peaks at 6.8°, 7.7°, 12.2°, 13.1°, 13.1°, 16.5°, 18.0°, 19.0°, 19.8° and 21.4° 2θ values while the drug loaded samples showed identical peaks with a significant reduced intensity. This was attributed to the small crystalline fraction on the silicon surface as previously determined by the DSC analysis. Furthermore, the pore loading is likely

to be responsible for the decrease in the peak intensities of the characteristic porous silicon peaks between 2° and 8° due to an increased electron density in the pores.

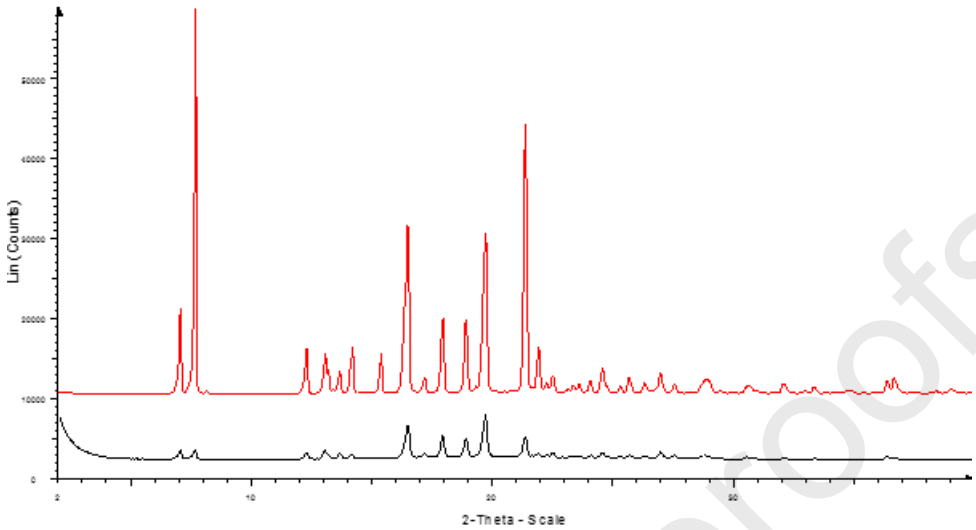

Fig. 5: Overlay XRD spectra of standard reference (S)-(+)-Ibuprofen and loaded (S)-(+)-Ibuprofen formulation

Both DSC and XRD suggest that the ibuprofen present in the pores of aerocrystals are crystalline in nature. This can be explained by the pore sizes of the adsorbent, the average pore size of aerocrystals used in the present study is 26 nm that can be particularly large for a comparatively small molecule such as ibuprofen. It has been previously stated that pore sizes 20 times or higher than the molecular radius can lead to crystallisation of the dug confined in pores [40]. The molecular dimensions of ibuprofen are approximately 1.3 X 0.6 nm that suggests 26 nm pore sizes to be sufficient large for drug to recrystallise upon solidification [41]. Similar observations were made for fenofibrate (molecular radius - ~1.27 nm), where it remained amorphous on the substrates with pores less than 20 nm but became crystalline when pore sizes increased above 20 nm [42].

3.2.2 EDX

Fig. 6 shows the SEM image of the cross-section of IBU-loaded sample, which, after oxidation, had a surface area of 415 m^2/g, pore volume of 2.52 cm^3/g and average pore diameter of 25.9 nm – again all reduced from the pre-oxidation values (Table 1). It was possible to detect the presence and distribution of the elemental carbon expected from IBU loading by fracturing the sample to reveal a freshly exposed surface in the cross-section. Five specific areas (25 x 25 µm) along the depth of the sample were probed by the electron beam to give an energy-

dispersive X-ray (EDX) analysis representation of the elements present in the layer. The EDX mapping is shown in Figure 7 and confirms a uniform distribution of carbon throughout the layer. The additional peaks are associated with elemental silicon (from the oxidised porous silicon) and oxygen (from the oxidised porous silicon and IBU).

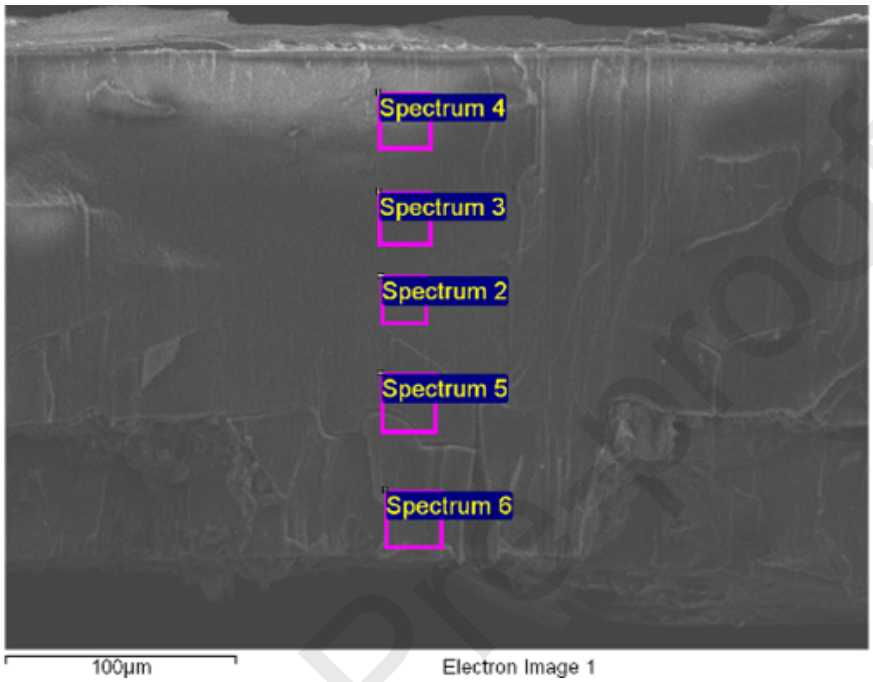

Fig. 6: Cross-sectional SEM image and EDX sampling points of a IBU-loaded aerocrystals

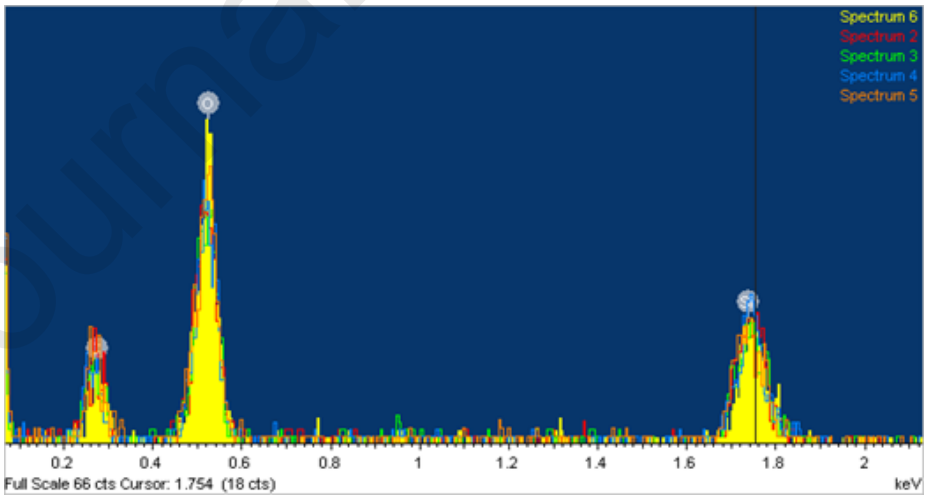

Fig. 7: Cross-sectional EDX spectra showing 'C' and 'O' after loading with (S)-(+)-Ibuprofen

3.3 *In-vitro* degradability

The *in-vitro* degradation of $scCO_2$-dried and air-dried aerocrystals is presented in Figure 8. $scCO_2$-dried flakes undergo significantly faster dissolution than air-dried equivalent that can be attribute to the their higher surface areas and pore volumes. Complete *in-vitro* dissolution of flakes was observed within 3 weeks, in contrast to air-dried controls that had only undergone about 20% dissolution over the same period.

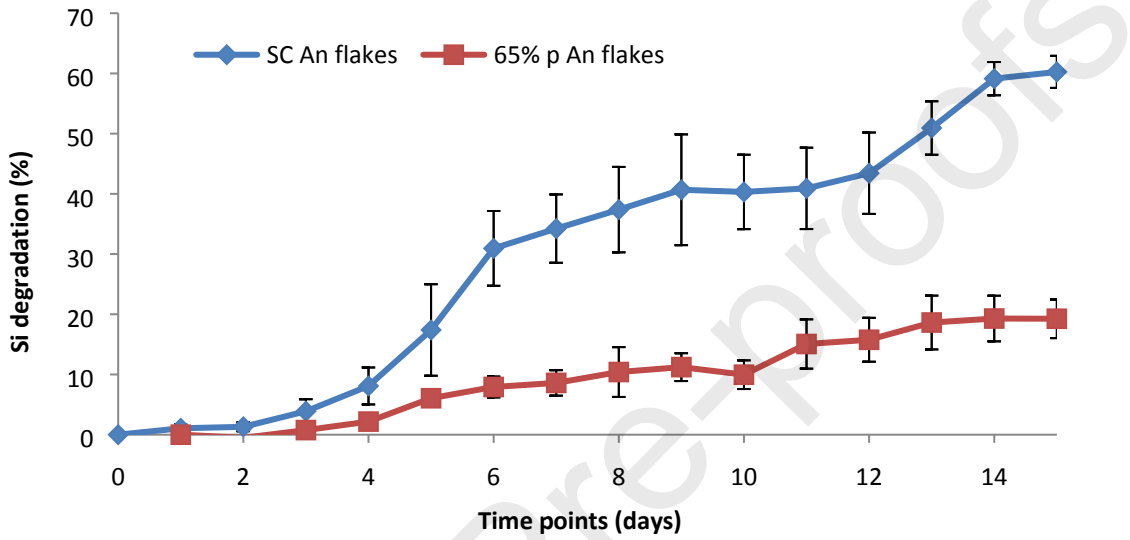

Fig. 8: *In-vitro* degradation of air-dried and $scCO_2$- dried porous silicon flakes in Tris buffer at pH 7.4 and 37°C (n=3)

3.4 Drug release from aerocrystals

In-vitro release of loaded IBU in pH 7.4 media undergoes an initial burst (Figure 9a) achieving about 65% release in 2 hours, that was much higher to the standard IBU dissolution of 15% at the same time (Figure 9a). The pKa of IBU is ~5.2 and its solubility in aqueous medium is strongly pH dependent. At acidic pH below or close to its pKa, the drug displays low aqueous solubility due to protonation of -COOH group which is evident from IBU dissolution as presented in Figure 9b. However, the IBU confined in the mesopores is less pH dependant thereby releasing faster from the matrix. This could be attributed to the formation drug nano-crystals formed in the pores that possess large surface area which aids to faster dissolution. The crystalline nature of the drug into the pores along with possibility of hydrogen bonding between the carbonyl group of IBU, and silanol groups on silica could be a reason behind the

incomplete release of the drug in the first two hours. It is possible that continuous and complete drug release could be obtained if this study is performed for longer.

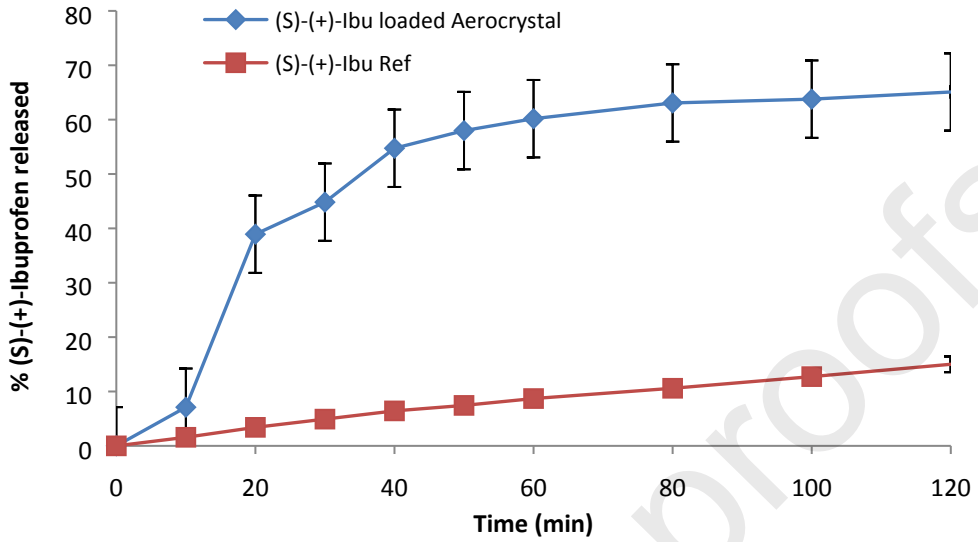

Fig. 9a: The release of IBU from porous aerocrystals and reference IBU in phosphate buffer pH 7.4 at 37 ^{o}C.

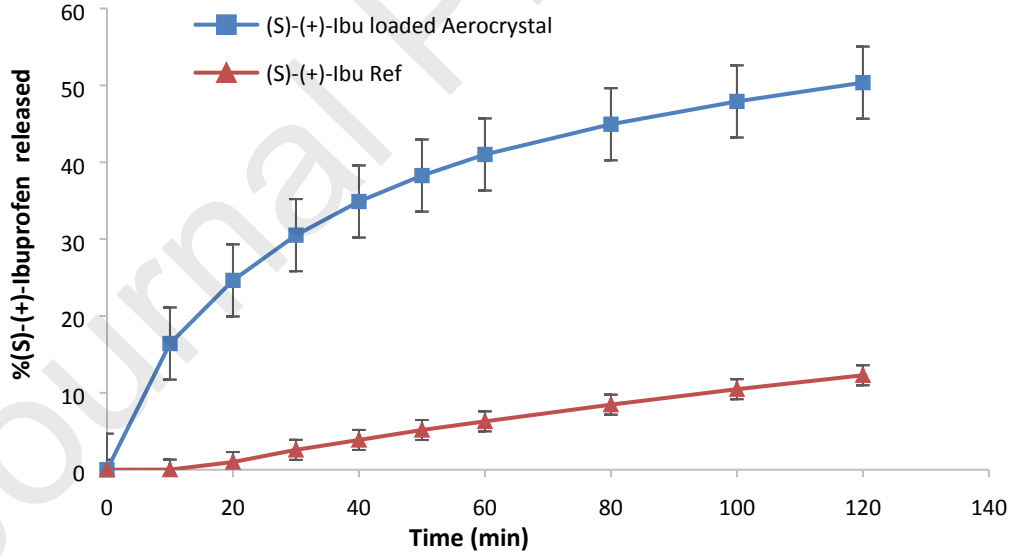

Fig. 9b: Overlay plot of release of (S)-(+)-Ibuprofen from porous silicon microparticles and dissolution of reference (S)-(+)-Ibuprofen in phosphate buffer pH 2.0 at 37^{o}C

Various dissolution models were applied to the release data (Table 4). Baker-Lonsdale [43] and Higuchi analysis [44] showed comparable least square regression values. Hence, it can be suggested that the drug release primarily occurs by counter-diffusion of media into the pores

of the aerocrystals, and release of drugs along with the solvent from the pores into the release media. These dissolution models clearly highlight the fact that IBU release is mainly due to the diffusion and not matrix erosion.

Table 4: Dissolution rate constants and determination coefficients of IBU release from aerocrystals.

Dissolution models		pH 7.4	pH 2
Baker and Lonsdale	k (hr^{-1})	$1.2x10^{-3} \pm 1.0x10^{-4}$	$5x10^{-4} \pm 1.8x10^{-5}$
	R^2	0.8905	0.9891
Zero order	k^0 (hr^{-1})	$0.755 \pm 5.3x10^{-2}$	$0.546 \pm 3.2x10^{-2}$
	R^2	0.3910	0.4809
First order	k_1 (hr^{-1})	$1.4x10^{-2} \pm 1.6x10^{-3}$	$8.0x10^{-3} \pm 1.3x10^{-3}$
	R^2	0.8072	0.7568
Higuchi	k_H ($hr^{-1/2}$)	7.02 ± 0.40	5.04 ± 0.16
	R^2	0.8587	0.9715
Hixson– Crowell	k_{HC} ($h^{-1/3}$)	$4.0x10^{-3} \pm 5.0x10^{-4}$	$2.4x10^{-3} \pm 2.0x10^{-4}$
	R^2	0.7148	0.6811
Peppas	k_P (hr^{-n})	10.57 ± 4.13	7.60 ± 0.73
	R^2	0.8775	0.9912
	n	0.403 ± 0.09	0.400 ± 0.02

Drugs falling under BCS class-II such as IBU have poor aqueous solubility. Various approaches have been utilised to improve the solubility of such drugs, one of which is to increase the specific surface area of the bulk active drug. To achieve adequate dissolution, smaller drug particles with higher equilibrium solubility are important. Melt loading of IBU in nanostructured pores leads to the formation of drug nanocrystals possessing high specific surface area. As shown in Fig. 9a, b the nanocrystalline form of the drug has greater solubility compared to reference IBU.

Another way to improve dissolution is to formulate amorphous forms of a drug molecule. Since there is no crystal lattice structure (no long-range order), the energy barrier to

dissolution is much reduced in amorphous solid forms. Classical nucleation theory suggests that crystal growth is favoured when nucleus of certain size r_{crt} surpasses a maximum free energy change ΔG_{Cryst}. The nuclei size smaller than r_{crt} will remain amorphous and not lead to crystallisation. Depending on the type of dissolution required, aerocrystal mesopores could be fine-tuned in such a way that these pores alter the dissolution of drug (e.g., by preventing or by assisting a drug molecule to reach r_{crt} level and hence by attaining a stable amorphous or nanocrystalline form within the pores). Analysing the dissolution data (Figure 9a & 9b), it is clear that pH dependency of the dissolution was reduced when IBU was loaded into the aerocrystals. It can be concluded that with poorly dissolving drugs, the loading into the mesoporous aerocrystals can clearly improve dissolution whilst also exhibiting very high payloads.

4. Conclusions

An important feature that a drug carrier should possess is the capability to carry a high drug payload. Supercritical drying of highly porous silicon aerocrystals has been shown to preserve very high surface areas and pore volumes compared to air-drying. The latter is crucial for maximising the internal payload of small drug molecules in mesoporous particles. We believe the drug loading achieved here is the highest internal payload reported to date for any complete mesoporous matrix-based delivery system, surpassed only by reservoir systems. Internal IBU loading exceeding 70 wt% was quantified by four different techniques and showed good agreement with theoretical predictions. It is also crucial for the drug carrier matrix to degrade, and high surface area achieved with $scCO_2$-drying promoted better wettability of the matrix thereby increasing the rate of degradation.

In conclusion, silicon-based mesoporous aerocrystals are not only medically degradable but have tuneable surface and pore properties capable of carrying very high drug payloads of poorly soluble drugs.

Conflicts of interest

There are no conflicts to declare.

Acknowledgements

The authors would like to thank E. Caffull, Q. Shabir, H. O' Brien and K. Webb for their kind contribution.

References

1. Vallet Regi et al. (2001) : A new property of MCM-41 : drug delivery system. Chem.Mater. 13(2) 308-311
2. Martin-Palma (2014) Nanostructured porous silicon-mediated drug delivery. Expert Opinion Drug Delivery 11(8) 1273-1283
3. I M.J.K. Thomas, I. Slipper, A. Walunj, A. Jain, M.E. Favretto, P. Kallinteri, D. Douroumis. Inclusion of poorly soluble drugs in highly ordered mesoporous silica nanoparticles. Int. J. Pharm. (2010), 387, 272 – 7
4. Andersson et al (2004) Influences of Material Characteristics on Ibuprofen Drug Loading and Release Profiles from Ordered Micro- and Mesoporous Silica Matrices. Chem. Mater. 16, 4160-4167
5. Hillerstrom et al. (2009) Ibuprofen loading into mesostructured silica using liquid carbon dioxide as a solvent. Green Chem. 11,662-667
6. Limnell et al. (2007) Surface chemistry and pore size affect carrier properties of mesoporous silicon microparticles. Int. J. Pharm. 343, 141-147
7. Wang et al. (2011) Ordered mesoporous carbons for ibuprofen drug loading and release behavior. Micropor. Mesopor. Mater. 142. 334-340
8. 1Smirnova I, Mamic J, Arit A. Adsorption of drugs on silica aerogels. Langmuir, 2003, 19(20) 8521-8525
9. Caputo (2013) Supercritical fluid adsorption of domperidone on silica aerogel. Adv. Chem. Engn. Sci. 3, 189-194
10. Alnaief M, Antonyuk S, Hentzschel C.M., Leopold C.S, Heinrich S, Smirnova I. A novel process for coating of silica aerogel microspheres for controlled drug release applications. Microporous and Mesoporous Materials 160 (2012) 167–173
11. P. Trucillo, S. Cardea, L. Baldino, E. Reverchon. Production of liposomes loaded alginate aerogels using two supercritical CO2 assisted techniques. J. CO2 Util. 39 (2020) 101161.
12. P. Trucillo, R. Campardelli, B. Aliakbarian, P. Perego, E. Reverchon, Supercritical assisted process for the encapsulation of olive pomace extract into liposomes, J. Supercrit. Fluids 135 (2018) 152–159,
13. R. Campardelli, P. Trucillo, E. Reverchon, Supercritical assisted process for the efficient production of liposomes containing antibiotics for ocular delivery, J. CO2 Util. 25 (2018) 235–241,
14. P. Trucillo, R. Campardelli, M. Scognamiglio, E. Reverchon, Control of liposomes diameter at micrometric and nanometric level using a supercritical assisted technique, J. CO2 Util. 32 (2019) 119–127,
15. P. Franco, I. De Marco. Supercritical CO2 adsorption of non-steroidal anti-inflammatory drugs into biopolymer aerogels. J. CO2 Util. 36 (2020) 40-53.
16. L. Goimil, V, Santos-Rosales, A. Delgado, C. Évora, R. Reyes, A.A.Lozano-Pérez, S.D.Aznar-Cervantes, J.L. Cenis, J.L. Gómez-Amoza, A. Concheiro, C. Alvarez-Lorenzo, C.A.García-González. scCO2-foamed silk fibroin aerogel/poly(ε-caprolactone)

scaffolds containing dexamethasone for bone regeneration. J. CO2 Util. 31 (2019) 51-64

17. L. Goimil, M.E.M. Braga, A.M.A. Dias, J.L. Gómez-Amoza, A. Concheiro, C. Alvarez-Lorenzo, H.C.de Sousa, C.A.García-González. Supercritical processing of starch aerogels and aerogel-loaded poly(ε-caprolactone) scaffolds for sustained release of ketoprofen for bone regeneration. J. CO2 Util. 18 (2017) 237-249.
18. R. Campardelli, P. Franco, E. Reverchon, I. De Marco, Polycaprolactone/nimesulide patches obtained by a one-step supercritical foaming+ impregnation process, J. Supercrit. Fluids 146 (2019) 47–54.
19. P. Franco, E. Reverchon, I. De Marco. Zein/diclofenac sodium coprecipitation at micrometric and nanometric range by supercritical antisolvent processing. J. CO2 Util. 27 (2018)366-373
20. L. Goimil, P. Jaeger, I. Ardao, J.L. Gómez-Amoza, A. Concheiro, C. Alvarez-Lorenzo, C.A. García-González, Preparation and stability of dexamethasone-loaded polymeric scaffolds for bone regeneration processed by compressed CO2 foaming, J. CO2 Util. 24 (2018) 89–98.
21. Yorov K.E., Kolesnik I.V., Romanova I.P., Mamaeva Yu. B, Sipyagin N.A., Lermontov N.A., Kopitsa G.P., Baranchikov A.E., Ivanov V.K. Engineering SiO2–TiO2 binary aerogels for sun protection and cosmetic applications. J. Supercr. Fluids (in press, https://doi.org/10.1016/j.supflu.2020.105099)
22. Posada L.F., Carroll M.K., Anderson A.M., Bruno B.A. Inclusion of Ceria in Alumina- and Silica-Based Aerogels for Catalytic Applications. J. Supercrit. Fluids, 2019, 152, 104536
23. Wang W., Zhou Y., Li Y., Hao T. Aerogels-filled Helmholtz resonators for enhanced low-frequency sound absorption. J. Supercrit. Fluids, 2019, 150, 103 – 111.
24. Babiarczuk B., Lewandowski D., Szczurek A., Kierzek K.,Meffert M., Gerthsenc D., Kaleta J., Krzak J. Novel approach of silica-PVA hybrid aerogel synthesis by simultaneous sol-gel process and phase separation. J. Supercrit. Fluids, 2020, 166, 104997.
25. Wu X., Wu Y., Zou W., Wang X., Du A., Zhang Z., Shen J. Synthesis of highly cross-linked uniform polyurea aerogels. J. Supercrit. Fluids, 2019, 151, 8-14.
26. Maximiano P., Durães L., Simões P.N. Organically-modified silica aerogels: A density functional theory study J. Supercrit. Fluids, 2019, 147, 138-148.
27. Nesterov N.S., Shalygin A.S., Pakharukova V.P., Glazneva T.S., Martyanov O.L. Mesoporous aerogel-like Al-Si oxides obtained via supercritical antisolvent precipitation of alumina and silica sols. J. Supercrit. Fluids, 2019, 149, 110-119.
28. Sanz-Moral L.M., Rueda M., Nieto A., Novak Z., Knez Z., Martín A. Gradual hydrophobic surface functionalization of dry silica aerogels by reaction with silane precursors dissolved in supercritical carbon dioxide. J. Supercrit. Fluids, 2013, 84, 74 – 79.
29. Ndayishimiye J., Popat A., Kumeria T., Blaskovich M. A.T., Falconer J.R. Supercritical carbon dioxide assisted complexation of benznidazole: γ-cyclodextrin for improved dissolution, Int. J. Pharm., 2021, 596, 120240.
30. Rudrangi S.R.S, Kaialy W., Ghori M.U., Trivedi V., Snowden M.J., Alexander B.D. Solid-state flurbiprofen and methyl-β-cyclodextrin inclusion complexes prepared using a single-step, organic solvent-free supercritical fluid process, Euro. J. Pharm. Biopharm., 2016, 104, 164-170.

31. Rudrangi S.R.S., Trivedi V., Mitchell J.C., Wicks S.R., Alexander B.D. Preparation of olanzapine and methyl-β-cyclodextrin complexes using a single-step, organic solvent-free supercritical fluid process: An approach to enhance the solubility and dissolution properties, Int. J. Pharm., 494 (1), 2015, 408-416.
32. Xu W., Zhao Z., Falconer J., Whittaker A. K., Popat A., Smith M.T., Kumeria T., Han F.Y. Sustained release ketamine-loaded porous silicon-PLGA microparticles prepared by an optimized supercritical CO2 process, Drug Deliv. and Transl. Res., 2021.
33. Canham et al (1994) Luminescent silicon aerocrystal networks prepared by anodisation and supercritical drying. Nature 368: 133-135
34. C.A. García-González, M.C. Camino-Rey, M. Alnaief, C. Zetzl, I. Smirnova. Supercritical drying of aerogels using CO2: effect of extraction time on the end material textural properties, J. Supercrit. Fluids 66 (2012) 297–306.
35. Sing K. (2001) The use of nitrogen adsorption for the characterisation of porous materials. Colloids & Surfaces A187-188, 3-9
36. Canham, (2014) Mechanical properties of porous silicon. In HANDBOOK OF POROUS SILICON Springer, Switzerland.
37. Iler (1979) Method of Analysis in THE CHEMISTRY OF SILICA. Wiley Interscience New York p94-104.
38. Brun M., Lallemand A., Quinson J.F., Eyraud C., (1977). A new method for simultaneous estimation of the size and the shape of the pore: The Thermoporometry. Thermochim. Acta, 21 p. 59.
39. J. Riikonen, E. Mäkilä, J. Salonen, V.P. Lehto. Determination of the physical state of drug molecules in mesoporous silicon with different surface chemistries. Langmuir 25 (2009) 6137–61.
40. Sliwinska-Bartkowiak, M., Dudziak, G., Gras, R., Sikorski, R., Radhakrishnan, R., Gubbins, K. Freezing behavior in porous glasses and MCM-41. Colloids Surf. A Physicochem. Eng. Asp. 2001, 187, 523–529.
41. Gonzalez G., Sagarzazu A., Zoltan T. Influence of Microstructure in Drug Release Behavior of Silica Nanocapsules, J. Drug Delivery, 2013, 2013 Article ID 803585.
42. Dwyer L.M., Michaelis V.K., O'Mahony M., Gri R.G., Myerson A.S. Confined crystallization of fenofibrate in nanoporous silica. Cryst. Eng. Comm. 2015, 17, 7922–7929.
43. Baker et al (1974) Controlled release: mechanisms and rates Controlled Release of Biologically Active Agents, Plenum Press, New York (1974), pp. 15–71.
44. Higuchi (1963) Mechanism of sustained-action medication. Theoretical analysis of rate of release of solid drugs dispersed in solid matrices. J. Pharm. Sci., 52 (1963), pp. 1145–1149.

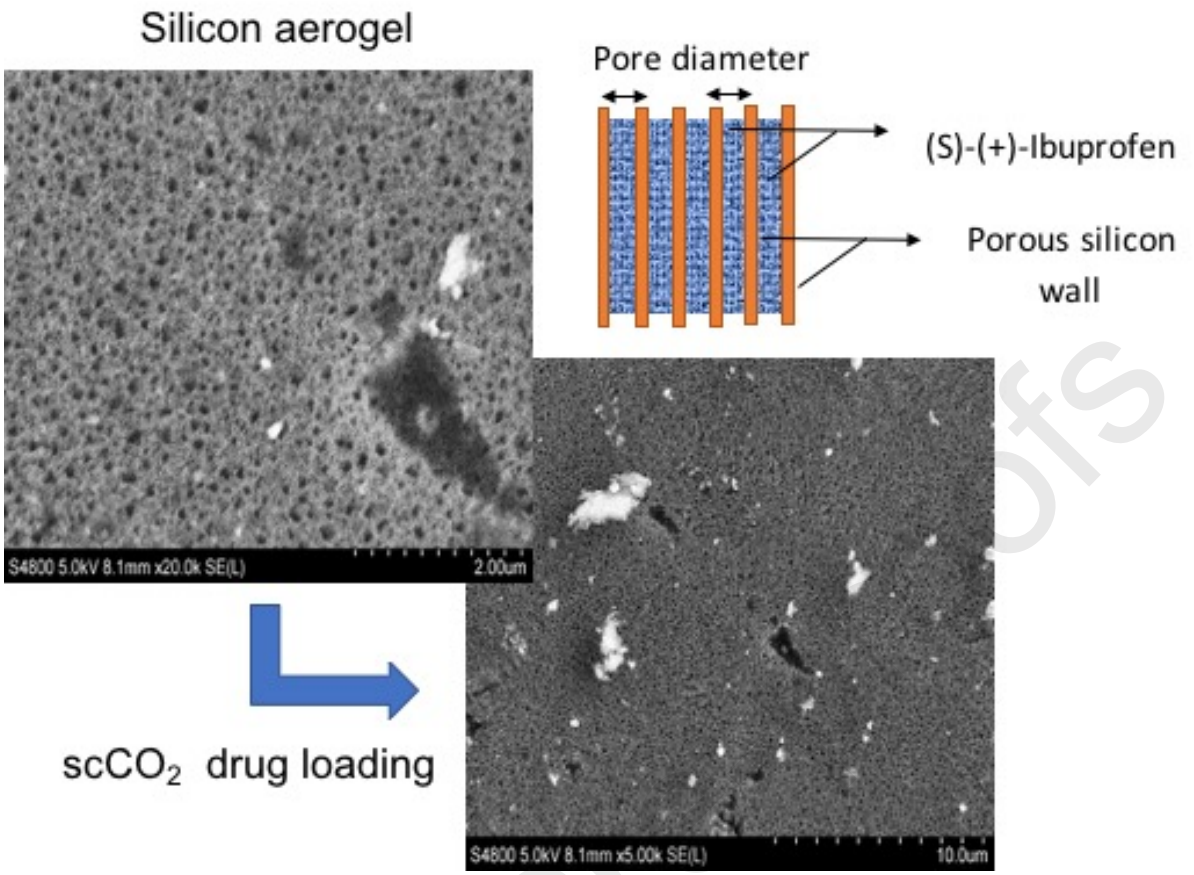

4 Credit authors statement

Conceptualization: Douroumis, Canham

Methodology: Canham, Loni, Nadarassan, Trivedi

Validation: Canham, Loni, Nadarassan, Trivedi

Formal analysis: Canham, Loni, Nadarassan

Investigation: Canham, Loni, Nadarassan, Trivedi, Douroumis

Writing - Original Draft: Canham, Nadarassan, Trivedi, Douroumis

Supervision: Canham, Trivedi, Douroumis

Project administration: Canham, Nadarassan

Declaration of interests

☒ The authors declare that they have no known competing financial interests or personal relationships that could have appeared to influence the work reported in this paper.

☐The authors declare the following financial interests/personal relationships which may be considered as potential competing interests: